On the Efficacy of ANSYS FLUENT in Predicting Transonic Flow Characteristics

Christopher Odetunde
Aeronautics and Astronautics Engineering Department
Kwara State University, Malete, Ilorin, Nigeria

Lucky Anetor
Department of Mechanical Engineering
Nigerian Defense Academy, Kaduna, Nigeria

Edward Osakue
Department of Industrial Technology
Texas Southern University, Houston, Texas

ABSTRACT

Transonic flows have long been studied. Our focus for this presentation is on the efficacy of an industrial CFD package/codes to the limit of its acceptability. Many companies use ANSYS FLUENT as their computational package, therefore, there is a need to check the efficacy of FLUENT, a CFD package in simulating a transonic NACA4412 airfoil. The airfoil geometric properties employed were: $a) Angle\ \ of\ attach,\ \alpha = 5^o$; $b)\ Mach\ \ number,\ Ma_\infty = 0.9$; c) Chord length, $c = 1.00m$; d) the specific heat at constant pressure, $C_p = 1006.43 J/(kg \cdot K)$, e) the thermal conductivity, $k = 0.242\ \ W/(m \cdot K)$, and f) the Spalart-Allmaras turbulence model usually reserved for aerospace application involving wall-bounded flows was used with: $c_{b_1} = 01355$; $c_{b_2} = 0662$; $c_{v_2} = 07$; $c_{v_2} = 0.3$. A full Multigrid (FMG) initialization was used to obtain better initial field flow variables. The solution was calculated using the pressure based coupled solver of the Fluent Computational Fluid Dynamics (CFD) package. Force and Surface monitors were used to check the solution convergence. The near-wall mesh resolutions were checked by plotting the distribution of the y^+ values. With a $Ma_\infty = 0.9$ (transonic), a fairly strong shock was observed near the trailing edge $(x/c = 0.87)$ on the upper (suction) surface of the airfoil. Reynolds number, *Re* based on the cord length of the airfoil was calculated to be 1.89×10^7. The convergence history of the airfoil performance parameters such as the average of surface vertex velocity, drag, lift, moment, pressure coefficients, etc. were computed.

Keywords: ANSYS Fluent, Spalart–Allmaras model, Transonic flows, Multigrid, Shockwave, Shock-capturing technique, upwind computational method.

Contact E-mail: chris.odetunde@kwasu.edu.ng

1. Nomenclature

Angle of attach	α
Freestream Mach number and Flow Mach number	M_∞, M_a
Chord length	c
Lift Coefficient	C_l
Drag Coefficient	C_d
Moment Coefficient	C_m
Pressure Coefficient	C_p
Pressure	P
Thermal Conductivity	k
Density	ρ
Laminar, Eddy viscosity	μ, μ_t
Functional relationship	$f_1, f_2, and\ f_3$
Momentum	M
Energy	E
Dynamic Pressure	$q,\ q_\infty = \frac{1}{2}\rho_\infty V_\infty^2$
Resultant force	R
Normal Force	N
Axial force	A
Area	S
y – plus	y^+
Wall shear stress	τ_w
A constant as long as α remains constant	Z
Lift	L

Drag	D
Dimensionless distance along the airfoil	x/c
Reynolds number	R_e
Flow velocities	u, v
Kinematic eddy (turbulent) viscosity	v_t
Vorticity Magnitude	S
Spalart Function	$f_{v2} = 1 - \frac{\chi}{1+\chi \cdot f_{v1}}$; $f_{v3} = 1$
σ	$\frac{2}{3}$
C_{b1}	0.1355
C_{b2}	0.622
κ	0.41
C_{w1}	$\frac{C_{b1}}{\kappa^2} + \frac{(1+C_{b2})}{\sigma}$
C_{w2}	0.3
C_{w3}	2
C_{v1}	7.1

ANSYS – is an Analysis System is a general purpose software, used to simulate interactions of all disciplines of physics, structural, vibration, fluid dynamics, heat transfer and electromagnetic for engineers.

NACA – The National Advisory Committee for Aeronautics (NACA)

Introduction

Several authors have studied flow over transonic airfoils. Murman, et. al. [1] studied a steady transonic flow past thin airfoils. The formulation involved using the small disturbance theory with non-linear mixed governing transonic potential differential equations. They formulated a boundary value problem and derived an analytical far field solution and were able to solve the transonic equation using mixed finite difference system to obtain cases with embedded shock waves. A non-lifting circular arc airfoils result was presented. A Nieuwland airfoil which agrees with experimental circular arc airfoils and exact theory for the shock free Nieuwland airfoil was investigated and the result was found to be excellent. Carlson [2, 3], on the other hand, developed an inverse solution technique for designing two-dimensional transonic airfoils by specifying pressure distribution on the airfoil. In his inverse method, Carlson found that the trailing edge displacement surfaces satisfying the input C_p distribution were not parallel, hence, invisicid solution was found to require a rear stagnation point behavior. Stratford [4], on the other hand, was able to predict the separation of the turbulent boundary layer. The flow structure over the wing of an aircraft is critical to its design. The same is true for other streamline bodies, for example, turbine blades, automobile shapes, propellers, etc. The performance of such bodies largely depends on the proper/accurate design of the shape of the airfoils constituting the relevant part(s) of the structure. Studies of airfoil characteristics, for example, lift versus Angle of Attack, Drag versus Angle of Attack, etc. show that there exists an optimal operating range [5, 6]. In view of this, the most important parameters that determine the performance of an airfoil namely, lift and drag forces will be calculated in this project. It is also worth mentioning that the use of numerical simulations have drastically reduced the cost of prototyping and experimentation. This has resulted in the concomitant advantage of savings in time, reduction in costs, and getting a product to the market before competitors.

In view of the foregoing, the purpose of this study is to investigate the efficacy of Fluent for a turbulent flow past a NACA4412 airfoil at a nonzero angle, $\alpha = 5^o$ of attack using the ANSYS Fluent version 12.1.4 Computational Fluid Dynamics (CFD) package. The Spalart-Allmaras turbulent model[1] was used [8, 9]. Spalart–Allmaras turbulence model was developed and designed for subsonic flow around airfoils. Spalart extended his model to subsonic and to transonic flows around aircraft configurations using its original [8]. The Spalart-Allmaras model is a relatively simple one-equation model that solves a modeled transport equation for the kinematic eddy (turbulent) viscosity, and a specification of a length scale by means of an algebraic formula and embodies a relatively new class of one-equation models in which, as stated above. Odetunde, et. al. [5] employed this model in the study of transonic NACA 4412 airfoil. For the Spalart-Allmaras one equation model, it is not necessary to calculate a length scale related to the local shear layer (boundary layer) thickness. The Spalart-Allmaras model was designed specifically for aerospace applications involving wall-bounded flows and the model is shown to give good results for boundary layers subjected to adverse pressure gradients [8, 9, 10, 11, 12, 13, 14, 15].

4.0 Goals and Objectives of this Study

The goals and objectives of present study are to: 1) Simulate compressible flow (using ideal gas law); 2) To determine if Fluent will correctly predict available NACA4412 data on the lift, drag and moment forces; 3) Employ Spalart-Allmaras turbulence model which is commonly used for aerospace fluid dynamics/aerodynamics problems; 4) Use Full Multigrid (FMG) initialization to obtain better initial field values; 5) Study the convergence criteria; 6) Use force and surface monitors to check solution convergence; and 7) Check near-wall mesh resolution by plotting the graph of y^+ in order to ascertain the orthogonality of the computational grid at the boundary.

5.0 Problem description and computational setup

Figure 1 shows NACA4412, the physical geometry under consideration. Figure two shows the numerical wind tunnel or computational field on which the solution to the transonic flow is to be obtained. In Figure 3 is a magnified view of the computational mesh showing that, at least, the grid having a smooth transition nearer the surface of the airfoil but a plot of α will provide a better assessment of the smoothness and orthogonality of the computational grid.

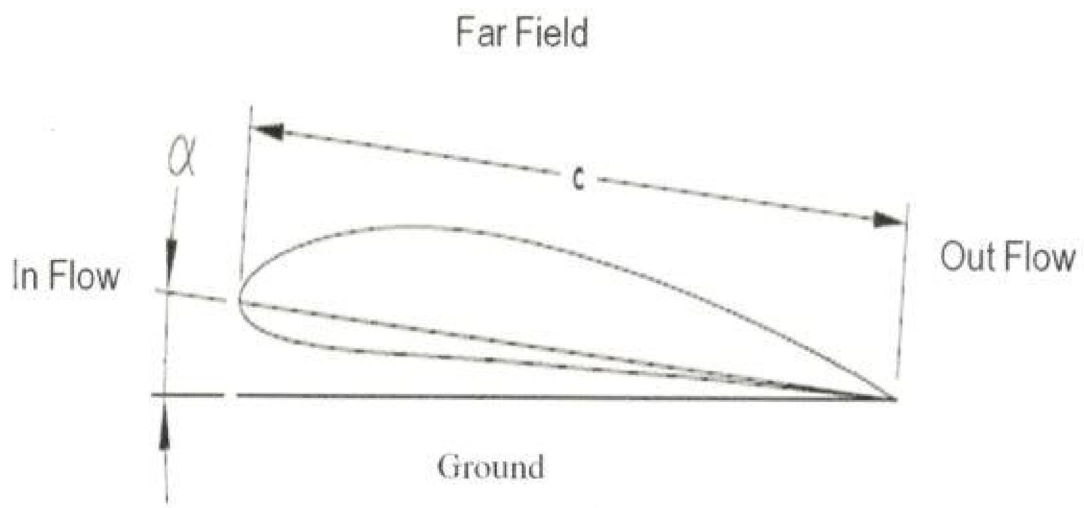

Figure 1: *NACA4412 airfoil showing at an angle of Attack,* $\alpha = 5^o$.

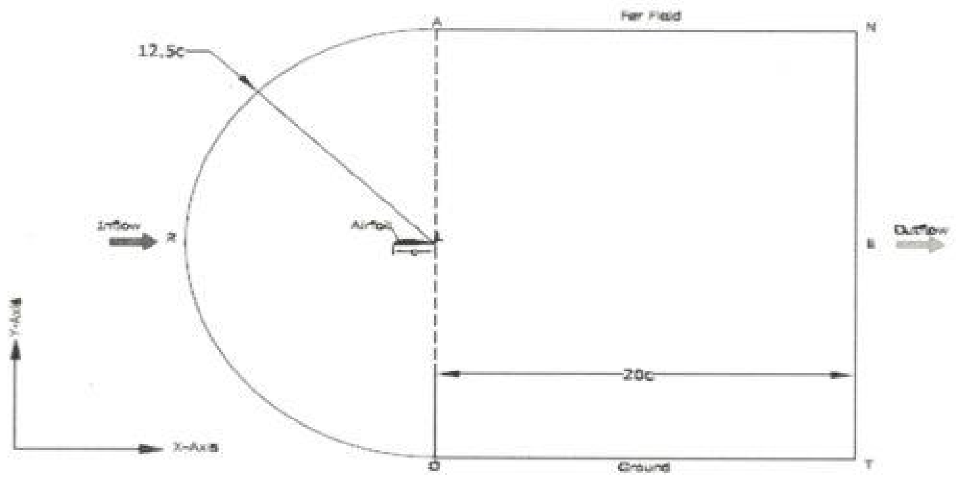

Figure 2: *Computational domain or "Numerical wind tunnel".*

5.1 Computational Mesh

The need to perform grid study is not always necessary in an industry setting because there are robust grid generation packages such as ICEM 3D, Plot3D, etc. (see Figure 3). For this study, ANSYS Fluent gridding package was employed. A C–Grid which better fits the type of computation domain and captures Far-Field boundary was employed as it has no discontinuity in slope and allows smooth mesh in the interior of the computational domain. For the grid and problem considered, the gradients normal to the airfoil wall are much greater than those tangential to the airfoil; therefore, the grids near the surface have high aspect ratios. For geometries that are more difficult to mesh, it may be easier to create a hybrid mesh consisting of quadrilateral and triangular grids.

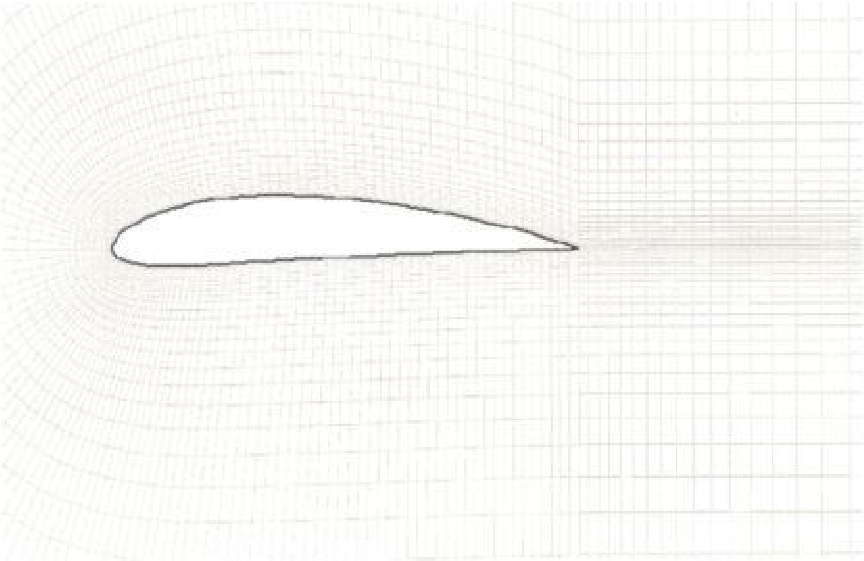

5.2 Bou

Figure 3: *Magnified view of the computational mesh around the airfoil.*

The boundary conditions are given in Table 1 below.

TABLE 1: Far-field Conditions

Fluid Property	**Numerical value**
Gauge Pressure (Pascal, Pa)	$0 \ Pa$
Freestream velocity in terms of Mach No., Ma_∞	$Ma_\infty = 0.9$
$x-component$ of Flow Direction	$\cos 5^o = 0.996195$
$y-component$ of Flow Direction	$\sin 5^o = 0.087156$
Temperature	$300 \ K$
Turbulent viscosity Ratio	10

5.3 Operating Conditions

The operating condition was set at 101325 Pa which is a reasonable and meaningful mean value for preventing any machine round-off errors.

5.4 Solution Methods and the solver

The Pressure-Based coupled algorithm was employed for the present computation because the pressure-based coupled solver is a good alternative to density-based solvers of **ANSYS FLUENT** when dealing with applications involving high-speed aerodynamics with shocks.

For the turbulence model, the one-Equation Spalart-Allmaras turbulence model was employed. The strain/vorticity-based and low-Reynolds damping production of the Spalart-Allmaras turbulence model were used to augment the turbulence model. The second-order upwind wind discretization scheme was chosen because it is capable of resolving the boundary layer and the shock effects more accurately than the first-order scheme. The transport equation for a working variable, $\overline{v}$, is given by:

$$\frac{\partial \widetilde{v}}{\partial t} + \overline{u}\frac{\partial \widetilde{v}}{\partial x_i} = \underbrace{c_{b1}\widetilde{S}\widetilde{v}}_{\text{Production}} + \frac{1}{\sigma}\left[\underbrace{\frac{\partial}{\partial x_j}\left((v+\widetilde{v})\frac{\partial \widetilde{v}}{\partial x_j}\right) + c_{b2}\frac{\partial \widetilde{v}}{\partial x_j}\frac{\partial \widetilde{v}}{\partial x_j}}_{\text{Diffusion}}\right] \underbrace{- c_{w1}f_w\left(\frac{\widetilde{v}}{d}\right)^2}_{\text{Destructioն}} \quad (1)$$

The eddy viscosity is defined as:

$$\mu_t = \overline{\rho}\widetilde{v}f_{v1} = \overline{\rho}v_t \quad (2)$$

In order to ensure that $\widetilde{v}$ is equal $\kappa y u_\tau$ in the log layer resident in the buffer layer and viscous sub-layer, a damping function, f_{v1}, defined by equation (3) was employed.

$$f_{v1} = \frac{\chi^3}{\chi^3 + c_{v1}^3}; \quad and \quad \chi = \frac{\widetilde{v}}{v} \quad (3)$$

Like Spalart et al., a modified vorticity magnitude, $\widetilde{S} = \frac{u_\tau}{\kappa y}$, is employed to maintain the log-layer behavior.

The modified vorticity is:

$$\widetilde{S} = f_{v3}\cdot\sqrt{2\Omega_{i,j}\Omega_{i,j}} + \frac{\widetilde{v}}{\kappa^2 d^2}f_{v2} \quad (4)$$

$$\Omega_{i,j} = \frac{1}{2}\left(\frac{\partial \widetilde{u}_i}{\partial x_j} + \frac{\partial \widetilde{u}_j}{\partial x_i}\right) \quad (5)$$

In the present study, the parameters for flow variables were set as shown in Table 1 above while the methodology for solving the equations are shown in Table 2.

TABLE 2: Solution Strategies Employed

Pressure-Velocity Coupling	**Coupled Scheme Solution Component of Fluent Chosen**

Spatial Discretization Scheme	*Least Square Cell – Based*
Gradient	*Standard*
Pressure	*Second – Order Upwind*
Density	*Second – Order Upwind*
Momentum	*Second – Order Upwind*
Modified Turbulent Viscosity	*Second – Order Upwind*
Energy	*Second – Order Upwind*

5.5 Solution Controls

A Courant number of 200 was found to be good enough for this analysis. An explicit relaxation factor of 0.5 was set for both the momentum and pressure. It is worth stating that under-relaxing the momentum and pressure variables is highly recommended for higher-order discretization schemes and under-relaxing the density variable is recommended for high-speed compressible flows. Recall that larger under-relaxation factors (that is, close to 1.0) will generally result in faster convergence but instability can occur when using large under-relaxation factors. However, the instabilities that result can be eliminated by decreasing the relevant relaxation factors.

For other flow variables, Table 3 shows the values of the under-relaxation factors:

TABLE 3: Under Relaxation Factors

Equation Variables	***Values***
Momentum	*0.5*
Forces	*1.0*
Modified Turbulent viscosity	*0.9*
Turbulent Viscosity	*1.0*
Energy	*1.0*

In order to monitor convergence as the calculations (iterations) progresses, the following residual quantities, namely, continuity, x-velocity, y-velocity and energy were monitored. The absolute convergence criteria which were set for these quantities are: $a)\ continuity = 0.001;$ $b)\ x-velocity = 0.001;\ \ c)\ \ y-velocity = 0.001;\ \ and$ d) for energy = $1.0e^{-6}$.

The solution was initialized and then the Full Multigrid (FMG) feature was run. Full Multigrid initialization often facilitates: a) an easier start-up thus obviating the need for a Courant-Friedrichs-Lewy (CFL) condition ramping; and b) The reduction in the number of iterations required for convergence. These strategies are important for implementing an industrial CFD code such as ANSYS FLUENT

6.0 Discussion of Results

Calculations were performed for 50 and 900 iterations. Figure 4 shows that the two velocity components and the thermal energy equation converged rapidly just before the tenth iteration. It can also be seen that the continuity equation shows this trend and attained a constant value at about the tenth iteration onwards. The turbulent kinetic energy, v_t, exhibits some oscillatory behavior between the second and twentieth iterations, thereafter, its oscillation decreased and tended to its converged solution.

Because fifty (50) iterations were found to be inadequate for all the relevant quantities for convergence, the iteration value was increased to 900. Figure 5 shows that all the relevant quantities, namely, the x and y components of velocity, the continuity, thermal and the turbulent kinetic energies attained converged from around two hundred and fifty (250) iterations onwards. It is pertinent to mention that all the quantities exhibited quite a few oscillations between initialization of computation up until the two hundred and fifty (250) iteration level.

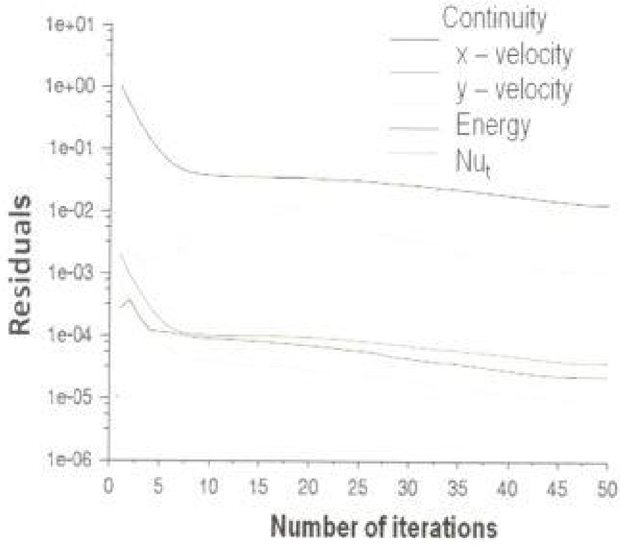

Fiqure 4: History of Residuals for 50 Iterations

Figure 4: *History of residuals for 50 iterations.*

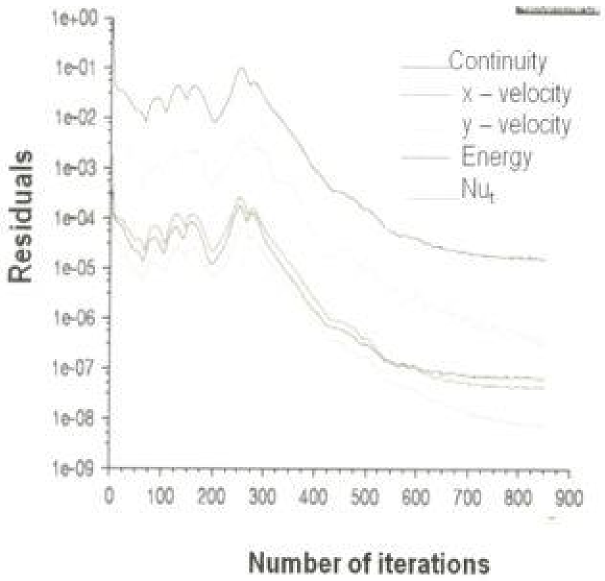

Figure 5: *History of residuals for 900 iterations.*

Figure 6 shows the convergence history of the velocity magnitude just downstream of the shock, $x/c \approx 0.87$ on the airfoil. It is worth mentioning that the drag, lift and moment coefficients are global variables amounting to certain overall averages, because of this, they may attain convergence while local quantities at specific points are still oscillating from one iteration to the next. It was in consideration of this type of observation that led to critically monitor the flow at a point, $x/c \approx 0.87$ just downstream of the shock where such significant variation was likely to be manifested.

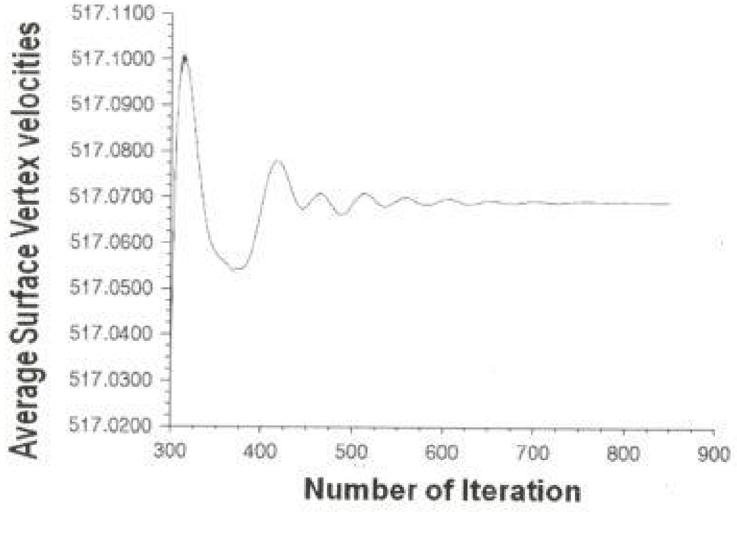

Figure 6: *Convergence history of velocity magnitude.*

In order to comprehensively discuss the results in Figures 7, 8 and 9 with respect to the efficacy of ANSYS FLUENT code, it would be appropriate to show the relationships between drag coefficient, C_d; lift coefficient, C_l, the moment coefficient, C_m for infinite/dimensionless wings; the Mach, M_o; and Reynolds number, *Re*.

6.1 Forces Acting on an Airfoil

During flight, a resultant force *R* acts on the wing. This force can be resolved into two forces in multiple ways. *R* can be resolved into *N* and *A*, where *N* is the component perpendicular (normal) to the chord, and *A* is the component tangential (axial) to the chord. However, *R* can also be resolved into a component *L* (lift) perpendicular to the relative wind, and *Drag, D* parallel to the relative wind. These forces have the following relation:

$$L = N\cos\alpha - A\sin\alpha \tag{6}$$

$$D = N\sin\alpha - A\cos\alpha \tag{7}$$

Applying similitude or dimensional analysis to infinite wing, we obtain the following relationship (refer to the nomenclature for definition of variables used here):

$$L = Z\rho_\infty V_\infty^2\left(\frac{1}{Ma_\infty}\right)^e\left(\frac{1}{\mathrm{Re}_c}\right)^f \tag{8}$$

The lift coefficient can also be written as follows:

$$C_l = \frac{L}{q_\infty S} = f_1(\alpha, Ma_\infty, \mathrm{Re}_c) \tag{9}$$

Repeating similar analysis for the drag, *D* and the moment, *M, can be obtained as:*

$$C_d = \frac{D}{q_\infty S} = f_2(\alpha, Ma_\infty, \mathrm{Re}_c) \tag{10}$$

$$C_m = \frac{M}{q_\infty S \cdot c} = f_3(\alpha, Ma_\infty, \mathrm{Re}_c) \tag{11}$$

Where $f_1, f_2, and\ f_3$ are functions of the parameters expressed in the parenthesis.

6.2 Lift

Figure 7 shows the convergence history of the lift coefficient. The figure shows a trend similar to those of the drag coefficient with higher values. The sharp drop in the value of the lift coefficient around the 280 iteration mark could be attributed to the sharp rise in fluid velocity arising from the shock observed at $x/c \approx 0.87$ (refer to Equation 9).

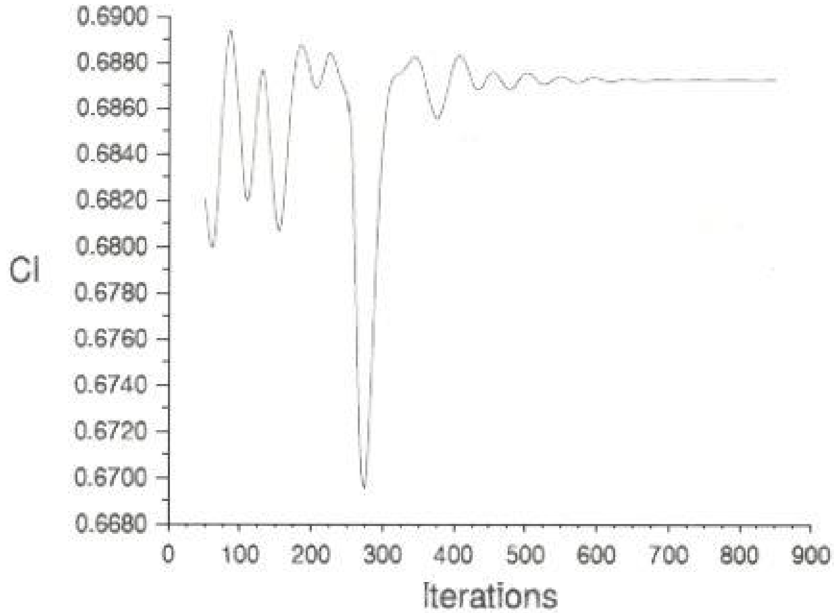

Figure 7: *Convergence behavior of drag coefficient,* c_l.

6.3 Drag

Figure 8 shows the convergence history of the drag coefficient also shows that there was a lot of oscillations before convergence was achieved after nearly 700 iterations. This observation is to be expected since the flow was fully turbulent. The sharp drop in the value of the drag coefficient at about the 280th iteration could be attributed to the location of shock observed at $x/c \approx 0.87$ (refer to Equation (10) above).

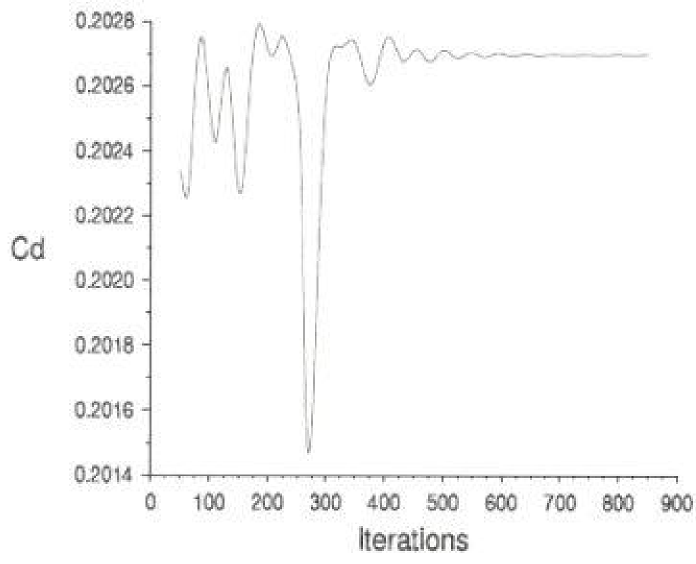

Figure 8: *Convergence behavior of Drag Coefficient,* C_d

6.4 Moment

In Figure 9, some oscillation was initially exhibited and thereafter, convergence was attained from around the 700 iteration. The sharp drop in the value of the moment coefficient around the 280 iteration mark could be attributed to the sharp rise in fluid velocity arising from the shock observed at $x/c \approx 0.87$ (refer to Equation 11).

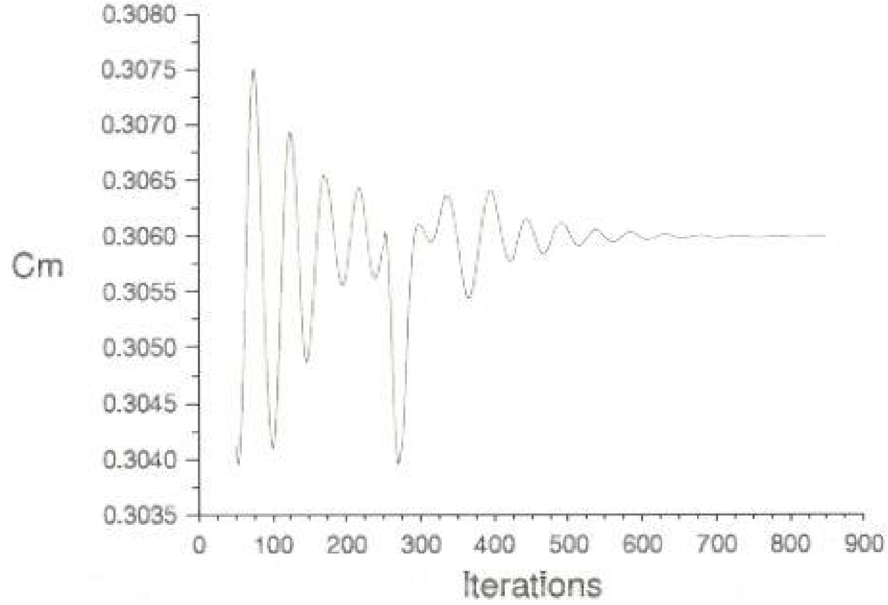

Figure 9: *Convergence behavior of Moment Coefficient,* C_m

Figure 10 shows the distribution of y^+. In order to discuss this figure effectively, it is pertinent to discuss the characteristics of y^+. The values of y^+ are dependent on the resolution of the mesh and the Reynolds Number of the flow and they are defined only in wall-adjacent cells. The value of $y+$ in the wall-adjacent cells dictates how wall shear stress is calculated. When the Spalart-Allmaras turbulence model is used, it is necessary to check that y^+ of the wall-adjacent cells is either very small (on the order of $y^+ = 1$), or approximately 30 or greater. Otherwise the computational mesh should be further refined. Equation (12) gives the formula for y^+ as:

$$y^{+} = \frac{y}{\mu}\sqrt{\rho \cdot \tau_{w}} \tag{12}$$

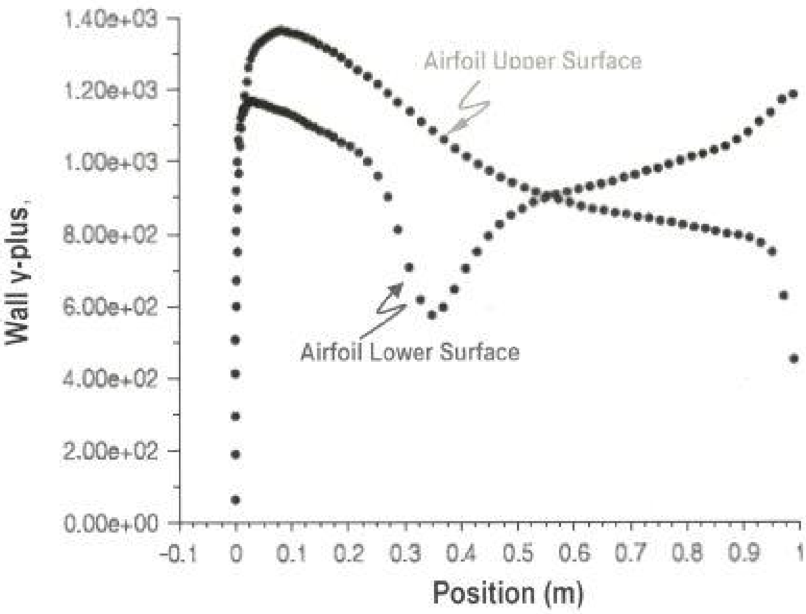

Figure 10: *Distribution of wall y-plus, y+*

As stated above, the pressure-based coupled solver and the Spalart-Allmaras
\ turbulence models were employed for this study. The y^{+} values were observed to be generally greater than 30 throughout the flow domain implying that the near-wall mesh resolution obtained was adequate. Thus one of the goals/objectives was achieved. The results of this exercise are captured and reported in Figures 4 to 16 and the features observed in the figures are clearly explained.

The pressure coefficient predicted the location of shock shown by experiment of wind tunnel result. Again, the upper shock location was found to be located at $x/c \approx 0.87$.

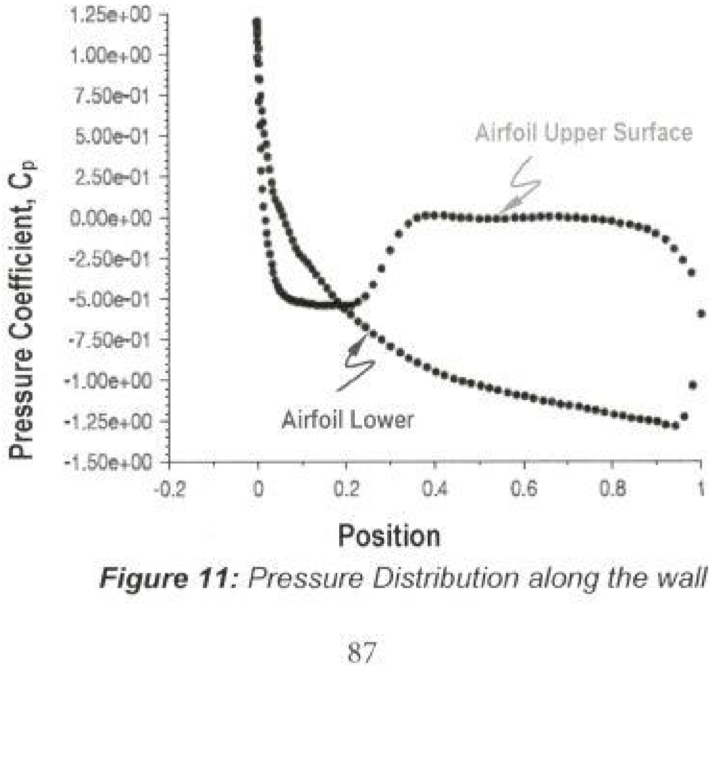

Figure 11: *Pressure Distribution along the wall*

Figure 12 shows the wall shear stress distribution along the surface of the airfoil. On the other hand, figure 13, provides the flow field distribution of Mach number. A plot of the velocity vector in the flow field also showed shock to be located at $x/c \approx 0.87$ on the pressure coefficient plot.

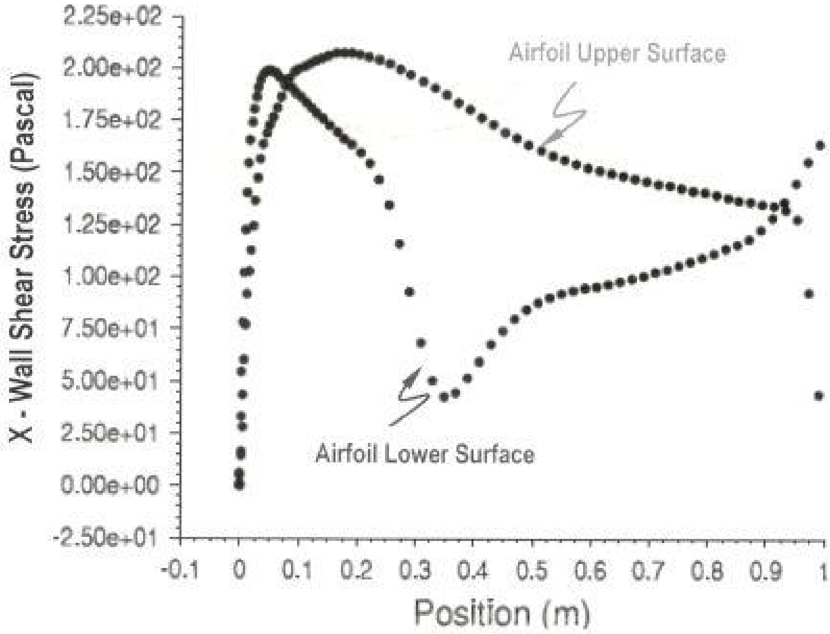

Figure 12: *Wall shear stress distribution along airfoil surface*

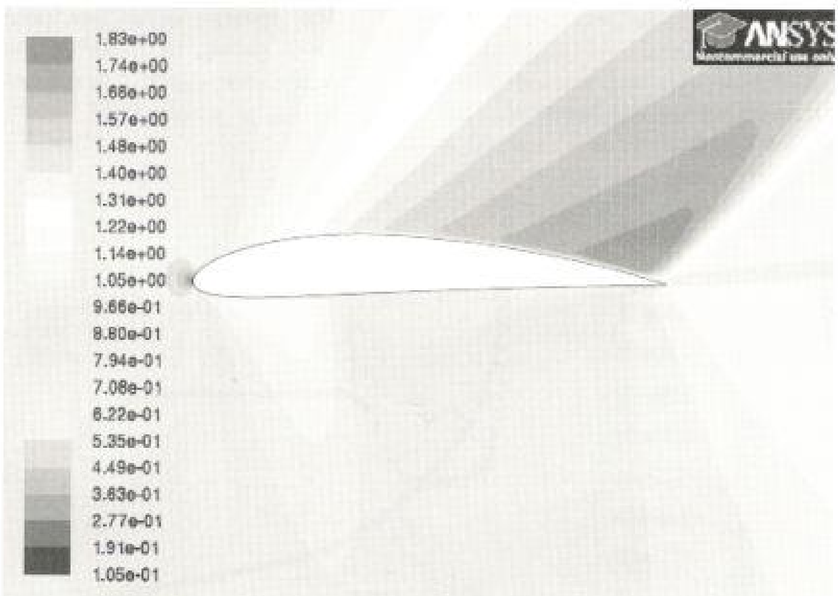

Figure 13: *Flow Field Mach number Contour*

7. Conclusion

A computational CFD package, ANSYS Fluent was employed to predict shock location, behavior of C_l, C_d, *and* C_m of a transonic airfoil and the efficacy of ANSYS FLUENT CFD in analyzing flow over Aerodynamic bodies. It has been successfully demonstrated that the Fluent CFD package is capable of predicting relevant flow parameters along the NACA4412 airfoil.

8. References

Murman, Earll M, and Cole, Julian D., "Calculation of Plane Steady Transonic Flows," Boeing Scientific Research Labs, Jan, 1970.

Carlson, L.A., "Transonic Airfoil Flow field Analysis Using Cartesian Coordinates," NANA CR – 2577, August 1975.

Carlson, L.A., "Inverse Transonic Flow Calculations Using Experimental Pressure Distribution," AIAA Journal, Vol. 12, No. 4, April 1974, pp. 571 – 572.

Stratford, B.S., "The Prediction of Separation of Turbulent Boundary Layer," Journal of Fluid Mechanics, Vol. 5, 1959, pp. 1 – 16.

Odetunde, C.B., Anetor, L, and Ishola, Y, "Modeling Turbulent Flow Past A NACA 4412 Airfoil," 10th Annual Oklahoma Aerospace Education Research Symposium, April 19 through April 22, 2011.

Bruce, P.J.K. and Babinsky, H. (2007) An experimental study of unsteady separated shock wave/boundary layer interactions In: 45th AIAA Aerospace Sciences Meeting and Exhibit, 8-11 January 2007, Reno, Nevada, USA.

Tucker, P.G. and Pan, Z. (2000) Turbulence modeling for unsteady flow complex systems in: Conference Proceedings of the 6th THERMINIC, 24-27 Sep 2000, Budapest, Hungary.

P.R. Spalart, S.R. Allmaras, A one equation turbulence model for aerodynamic flows, AIAA Paper 92-0439, 1992.

P.R. Spalart, S.R. Allmaras, A one equation turbulence model for aerodynamic flows, in: La Recherche Aérospatiale, 1994, pp. 5–21.

C. Gacherieu, C. Weber, Assessment of algebraic and one-equation turbulence models for transonic turbulent flow around a full aircraft configuration, AIAA Paper 98-32457, 1998.

Dacles-Mariani, J., Zilliac, G. G., Chow, J. S. and Bradshaw, P. (1995), Numerical/Experimental Study of a Wingtip Vortex in the Near Field, AIAA Journal, 33(9), pp. 1561-1568, 1995.

Shur, M. L., Strelets, M. K., Travin, A. K., Spalart, P. R., "Turbulence Modeling in Rotating and Curved Channels: Assessing the Spalart-Shur Correction," AIAA Journal Vol. 38, No. 5, 2000, pp. 784-792.

Eca, L., Hoekstra, M., Hay, A., and Pelletier, D., A Manufactured Solution for a Two-Dimensional Steady Wall-Bounded Incompressible Turbulent Flow, International Journal of Computational Fluid Dynamics, Vol. 21, Nos. 3-4, 2007, pp. 175-188.

Aupoix, B. and Spalart, P. R., Extensions of the Spalart-Allmaras Turbulence Model to Account for Wall Roughness, International Journal of Heat and Fluid Flow, Vol. 24, 2003, pp. 454-462.

Rung, T., Bunge, U., Schatz, M., and Thiele, F., Restatement of the Spalart-Allmaras Eddy-Viscosity Model in Strain-Adaptive Formulation, AIAA Journal, Vol. 41, No. 7, 2003, pp. 1396-1399.

S. V. Patankar, "Numerical Heat Transfer and Fluid Flow, Hemisphere," Washington, D.C (1980).